Effect of bioink properties on printability and cell viability for 3D bioplotting of embryonic stem cells

2016 Biofabrication 8 035020

(http://iopscience.iop.org/1758-5090/8/3/035020)

Biofabrication

PAPER

Effect of bioink properties on printability and cell viability for 3D bioplotting of embryonic stem cells

Liliang Ouyang[1,2], Rui Yao[1,2], Yu Zhao[1,2] and Wei Sun[1,2,3]

[1] Biomanufacturing Center, Department of Mechanical Engineering, Tsinghua University, Beijing 100084, People's Republic of China
[2] Biomanufacturing and Rapid Forming Technology Key Laboratory of Beijing, Beijing 100084, People's Republic of China
[3] Department of Mechanical Engineering, Drexel University, Philadelphia, PA 19104, USA

E-mail: yaorui@tsinghua.edu.cn

RECEIVED
13 May 2016

REVISED
24 July 2016

ACCEPTED FOR PUBLICATION
31 August 2016

PUBLISHED
16 September 2016

Keywords: 3D cell printing, embryonic stem cells, printability, viability, bioink properties, bioprinting

Supplementary material for this article is available online

Abstract

3D cell printing is an emerging technology for fabricating complex cell-laden constructs with precise and pre-designed geometry, structure and composition to overcome the limitations of 2D cell culture and conventional tissue engineering scaffold technology. This technology enables spatial manipulation of cells and biomaterials, also referred to as 'bioink', and thus allows study of cellular interactions in a 3D microenvironment and/or in the formation of functional tissues and organs. Recently, many efforts have been made to develop new bioinks and to apply more cell sources for better biocompatibility and biofunctionality. However, the influences of printing parameters on the shape fidelity of 3D constructs as well as on cell viability after the cell printing process have been poorly characterized. Furthermore, parameter optimization based on a specific cell type might not be suitable for other types of cells, especially cells with high sensibility. In this study, we systematically studied the influence of bioink properties and printing parameters on bioink printability and embryonic stem cell (ESC) viability in the process of extrusion-based cell printing, also known as bioplotting. A novel method was established to determine suitable conditions for bioplotting ESCs to achieve both good printability and high cell viability. The rheological properties of gelatin/alginate bioinks were evaluated to determine the gelation properties under different bioink compositions, printing temperatures and holding times. The bioink printability was characterized by a newly developed semi-quantitative method. The results demonstrated that bioinks with longer gelation times would result in poorer printability. The live/dead assay showed that ESC viability increased with higher printing temperatures and lower gelatin concentrations. Furthermore, an exponential relationship was obtained between ESC viability and induced shear stress. By defining the proper printability and acceptable viability ranges, a combined parameters region was obtained. This study provides guidance for parameter optimization and the fine-tuning of 3D cell printing processes regarding both bioink printability and cell viability after bioplotting, especially for easily damaged cells, like ESCs.

1. Introduction

As an emerging approach focused on establishing biomimetic and functional tissue-like constructs in three-dimensions, 3D cell printing is a rising technology for a variety of applications including tissue engineering, regenerative medicine, drug testing and screening, physiological/pathological modeling, and other biological studies [1]. By using a computer-controlled 3D printing device, cell printing technology can manipulate cells together with growth factors and biomaterials based on a pre-designed computer model. Compared to the scaffold-based strategy, cell printing technologies overcome the limitations of low cell delivery efficiency and uncontrolled cell/biomaterials distribution by controlled deposition of cell-laden 'bioinks', which might be hydrogels, viscous fluids, or microcarriers [2]. There are four basic approaches to conduct cell printing: inkjet- [3], extrusion- [4], acoustic- [5] and laser-based [6],

among which the extrusion method, also known as 'bioplotting', demonstrates the advantages of additive manufacturing to the largest extent by creating real 3D macro constructs through appropriate extrusion and crosslinking of bioinks. Physically, inkjet-, acoustic- and laser-based methods could be categorized as jet-based cell printing, which generates and deposits bioink droplet by using thermal, piezoelectric, acoustic, laser and pneumatic energies [1]. Although capable of ejecting droplets of picolitre volume while simultaneously achieving high deposition resolution, jet-based cell printing technologies can be time-consuming due to the droplet size and be limited to materials with low viscosity, thus making it difficult to fabricate large-scale tissue-like products with good mechanical properties.

Bioink development, characterization and parameter optimization are of great importance in bioplotting, since bioink properties play an essential role in both the fabrication of integrated layer-by-layer constructs and the formation of functional tissues or organs. Physically, bioinks should exhibit gelation characteristics after extrusion from a nozzle tip and demonstrated a solidified filament morphology which should be mechanically strong enough to support the deposition of upper layers [7]. Physiologically, bioinks should offer suitable microenvironments to support various cell activities, like migration, proliferation, differentiation and specific tissue generation. Bioink printability, namely the ability to form 3D structure with good fidelity and integrity, and cell viability, namely cell survival rate post printing, are viewed as primary representative criteria of the physical and physiological properties, respectively. There are many studies to evaluate bioinks and optimize parameters that aim at these two criteria by using different printing methods, biomaterials and cell types. Murphy *et al* [8] systematically evaluated the gelation time, swelling or contraction, stability, biocompatibility and printability of twelve hydrogels, including collagen, fibrin, alginate etc. Chung *et al* [9] applied various analytical techniques to explore the printability of pre-crosslinked alginate and alginate/gelatin blended inks in an extrusion-based printing system, finding that printability was enhanced by adding gelatin. Nair *et al* [10] characterized the viability of endothelial cells during extrusion-based printing and the results indicated that dispensing pressure had a more significant effect on cell viability than the nozzle diameter. Hendriks *et al* [11] developed a model to connect rat fibroblasts survival with cell-containing droplet size and velocity, and the substrate properties in a droplet-based deposition system. Catros *et al* [12] founded that lower laser energy, thicker substrate films and higher bioink viscosity contributed to a higher survival rate of endothelial cells in laser-assisted printing. In a study of 3D printing HEK 293FT cells with a gelatin-based hydrogel, it was found that nozzle insulation greatly improved cell viability after the printing process [13].

All of the above studies were focused on the influence of bioink properties and printing parameters on either bioink printability or cell viability. However, to achieve a successful 3D cell printing procedure, all parameters need to be carefully tuned to ensure both good printability and high cell viability. Otherwise, either the 3D cell-laden construct may lose printing accuracy and/or structural integrity during long-term culture, or the cells may undergo apoptosis and/or experience a change of phenotype. Recently, Zhao *et al* demonstrated that bioink viscoelasticity was the decisive factor for both printability and cancer cell viability when other process parameters, i.e. printing speed and extrusion flux, remained constant [14]. They also mentioned that, for different embedded cells, different viscoelastic range might be needed. Blaeser *et al* [15] chose shear stress as a key factor against which to balance printing resolution and cell integrity in a valve-based jet printing process. They found that shear stress should be controlled within 5 kPa to obtain more than 90% living cells for mouse fibroblasts.

Unlike the above mentioned mature cells or cell lines, embryonic stem cells (ESCs), with the capabilities of unlimited self-renewal and of differentiating into all the cell types in mammals, hold unique promise as a robust cell source for tissue engineering, regenerative medicine, drug testing, and biology study applications. However, as a powerful cell source, ESCs, especially human ESCs, are critically sensitive to changes in cellular microenvironment, e.g. disassociation, temperature, shear stress, and even illumination [16, 17]. Recently, we successfully embedded mouse ESCs into a cell-laden 3D construct via extrusion-based cell printing technology for the first time, while maintaining ESC proliferation and pluripotency, and achieving controllable and uniform embryoid body formation [18]. To our knowledge, there is no report about parameter optimization or about the study of bioink properties to achieve both high cell viability and good printability for 3D printing of ESCs.

In this study, we aimed to explore the influence of bioink properties on ESC viability as well as bioink printability, and to establish a methodology for optimizing printing parameter ranges for 3D printing of ESCs. An extrusion-based 3D cell printer with a temperature-controlled nozzle and printing chamber was used to fabricate cell-laden constructs with interconnected channels, which facilitated mass transfer of oxygen and nutrients. A gelatin/alginate mixture bioink was used for its ease of gelation and its cytocompatibility [19, 20]. Bioink concentration, printing temperature and holding time were taken into consideration as three basic printing parameters. The evaluation of bioink printability was performed by introducing a semi-quantitative approach based on rheological measurements and image analysis. Cell viability was characterized based on live/dead staining and was fitted as a function of induced shear stress. Lastly, a suitable range of parameter configurations

was obtained considering the balance between bioink printability and cell viability. The approaches developed in this study provide criteria and tools by which printability and viability can be evaluated and proper printing parameters can be chosen for extrusion-based cell printing of all kinds of cells, including pluripotent stem cells.

2. Materials and methods

2.1. Cell culture

Undifferentiated mouse ESCs (R1 cell line, a kind gift from Prof Na Jie's group in the Center for Stem Cell Biology and Regenerative Medicine, Tsinghua University, China) were cultured in DMEM (Gibco, 11960-044) supplemented with 15% knock out TM SR serum replacement for ESC/iPSCs (Gibco, 10828-028), 0.1 mM MEM non-essential amino acids (Gibco, 11140-050), 2 mM GlutaMax-1 (Gibco, 35050-061), 1 mM sodium pyruvate (Gibco, 11360-070), 100 U ml^{-1} penicillin/streptomycin (Gibco, 10378-016), 1000 U ml^{-1} leukemia inhibitory factor (ESGRO, ESG1106) and 0.1 mM β-mercaptoethanol (SIGMA, M-3148). Cells were passaged every 2 to 3 days with 0.025% trypsin/EDTA onto 0.1% gelatin-coated Petri dishes.

2.2. Bioink preparation

Gelatin (type A from porcine skin, Sigma-Aldrich, G1890) and alginic acid sodium salt powder (Sigma-Aldrich, A0682) were dissolved in 0.5% sodium chloride solution as storage bioink solutions. The bioink solutions were sterilized by heating at 70 °C for 30 min three times, and then stored in 4 °C before usage. Mycoplasma detection was carried out using a GMyc-PCR Mycoplasma Test Kit (YEASEN, 40601ES20) to avoid mycoplasma contamination. After incubation in 37 °C for 30 min, the gelatin solution, alginate solution and ESC suspension were gently and evenly mixed at specific ratios to prepare bioinks with final concentrations of 5%/7.5%/10% (w/v) gelatin, 1% (w/v) alginate and 1×10^6 ESCs cells ml^{-1}, respectively. Bioink mixtures of 5% gelatin plus 1% alginate, 7.5% gelatin plus 1% alginate, and 10% gelatin plus 1% alginate were termed as 5% Gel + 1%Alg, 7.5%Gel + 1%Alg, and 10% Gel + 1%Alg, respectively. All materials and reagents were purchased from Invitrogen unless otherwise stated.

2.3. Rheological measurement

Rheological measurements were performed using a Physica MCR 302 rheometer (Anton Paar, Germany) with a cone-plate geometry measuring system (25 mm diameter, 2° cone angle, 99 truncation gap). The storage modulus (G'), loss modulus (G'') and complex viscosity ($|\eta^*|$) were recorded as a function of time through oscillatory measurements under a strain of 0.1% and frequency of 1.5 Hz, unless otherwise stated. These conditions were confirmed to be in the linear viscoelastic region. In addition, temperature sweep oscillatory tests were also tested through cooling or warming processes with the rate of 5 °C min^{-1}. As shown in the schematic (figure 1), the bioinks were incubated in 37 °C before testing and the temperature-controlled testing plate was also set at 37 °C as an initial temperature. The time dependence of G' and G'' of gelation solutions with different concentration (5%, 7.5% and 10%) were measured according to different measurement temperature (22.5 °C, 25 °C, 27.5 °C and 30 °C). The measurement temperature setting corresponded to the setting of the printing temperature. The gelation time (t_{gel}) was calculated as the time at which G' intersected G''.

2.4. Cell printing process

The bioinks were printed using an extrusion-based 3D cell printer following previously established methods [13]. Briefly, through the temperature-controlled nozzle, printing temperature was set at 22.5 °C, 25 °C, 27.5 °C and 30 °C, referred to as PT-22.5 °C, PT-25 °C, PT-27.5 °C and PT-30 °C, respectively. The printing chamber was held at 22.5 °C, which is near room temperature to facilitate immediate gelatin crosslinking and 3D construct formation. A two-layered grid construct with the layer distance of 150 μm was printed with an extrusion flux of 0.68 μl s^{-1} and a stainless steel needle gauge of 25 G, unless otherwise stated. After printing, the cell-laden constructs were immersed in 100 mM calcium chloride for 3 min for crosslinking, washed with phosphate buffer solution (PBS) for three times, and then cultured with ESC culture medium. Culture medium was changed every 1∼2 days.

2.5. Semi-quantification of printability

When the bioink was in an ideal gelation condition, the extruded filament would demonstrate a clear morphology with smooth surface and constant width in three dimensions, which would result into regular grids and square holes in the fabricated constructs. When the bioink was in an under-gelation condition, the extruded filament would demonstrate a more liquid-like state, and the upper layer would fuse with the lower layer, thus creating approximately circular holes. As we know, circularity (C) of an enclosed area is defined as the following

$$C = \frac{4\pi A}{L^2}, \tag{1}$$

where, L means perimeter and A means area. Circles have the highest circularity ($C = 1$). The closer the C value is to 1, the closer the shape is to a circle. For a square shape, circularity is equal to $\pi/4$. We defined the bioink printability (Pr) based on square shape using the following function

$$\mathrm{Pr} = \frac{\pi}{4} \cdot \frac{1}{C} = \frac{L^2}{16A}. \quad (2)$$

For an ideal gelation condition or perfect printability status, the interconnected channels of the constructs would demonstrate square shape, and the Pr value was 1. The larger the Pr value was, the greater the gelation degree of the bioink was determined to be. The smaller the Pr value was, the smaller the gelation degree the bioink was. To determine the Pr value of each printing parameter combination, optical images of printed constructs were analyzed in Image-Pro-Plus software to determine the perimeter and area of interconnected channels ($n = 5$).

2.6. Live/dead staining

Fluorescent live/dead staining was used to determine cell viability in the 3D cell-laden constructs according to the manufacturer's instructions. Briefly, samples were gently washed in PBS 3 times. 1 μM Calcein-AM (Sigma-Aldrich, 17783) and 2 μM propidium iodide (Sigma-Aldrich, P4170) were used to stain live cells (green) and dead cells (red), respectively, during 15 min incubation while avoiding light. A laser scanning confocal microcopy system (LSCM, Nikon, Z2) was used for image acquisition. Cell viability was counted with the count/size tool of Image-Pro-Plus and calculated by dividing the total number of cells by green stained cells. Three random fields were counted for each sample.

2.7. Shear stress determination

Shear stress at the needle site was estimated to evaluate its influence on cell viability. For a non-Newtonian fluid, the shear stress (τ) can be given by a power-law function in equation (3) [21]:

$$\tau = \eta\dot{\gamma} = K\dot{\gamma}^{n}, \quad (3)$$

where η is the viscosity of non-Newtonian fluid, $\dot{\gamma}$ is the shear rate, K is the consistency index, which is determined by material concentration and temperature, and n is the power law index or flow behavior index. Meanwhile, the viscosity can be given by equation (4):

$$\eta = K\dot{\gamma}^{n-1}. \quad (4)$$

To calculate shear stress, shear rate was determined by assuming a laminar fluid (figure S1), while the indices K and n were determined experimentally via flow tests by using equation (4), as sated in supporting information.

2.8. Statistical analysis

All results were presented as the mean ± standard deviation (SD). Statistical analysis was performed by GraphPad Prism using one-way analysis of variance (ANOVA) in conjugation with a Bonferroni *post-hoc* test. Statistical significance was defined as $^{*}p < 0.05$, $^{**}p < 0.01$, $^{***}p < 0.001$. Three independent trials were carried out unless otherwise stated.

3. Results

3.1. Rheological evaluation of bioink

The rheological properties of bioinks with different compositions were assessed by rheological measurements. As shown in figure 2(A), the viscosity of the 7.5% gelatin solution (7.5%Gel) increased sharply when temperature was less than 25 °C. On the other hand, the viscosity of the 1% alginate solution (1%Alg) changed little with temperature, suggesting that alginate was not temperature-responsive. Besides, the rheological properties of the gelatin/alginate mixtures were similar to gelatin solutions, suggesting that the gelatin component played a more important role in the thermal gelation of the mixture. Furthermore, the rheological behavior of gelatin/alginate mixture differed between cooling and warming processes

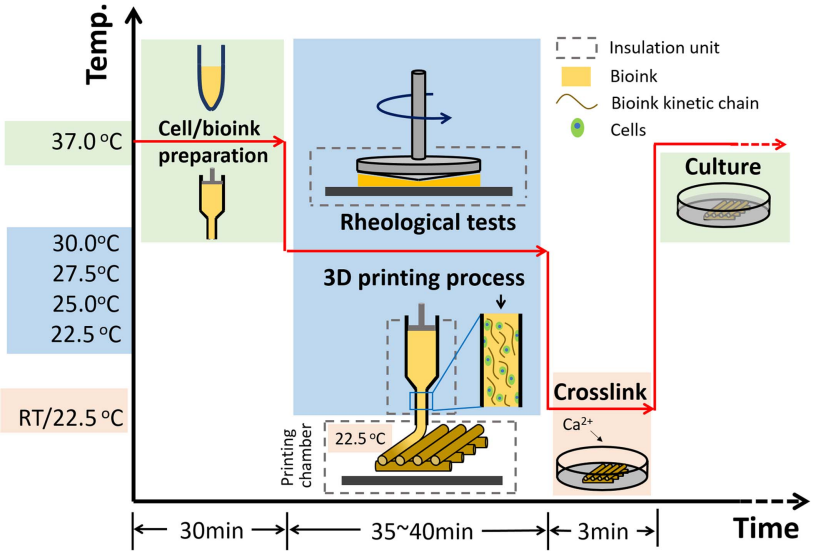

Figure 1. Schematic of the study indicated the temperature and time at different sections.

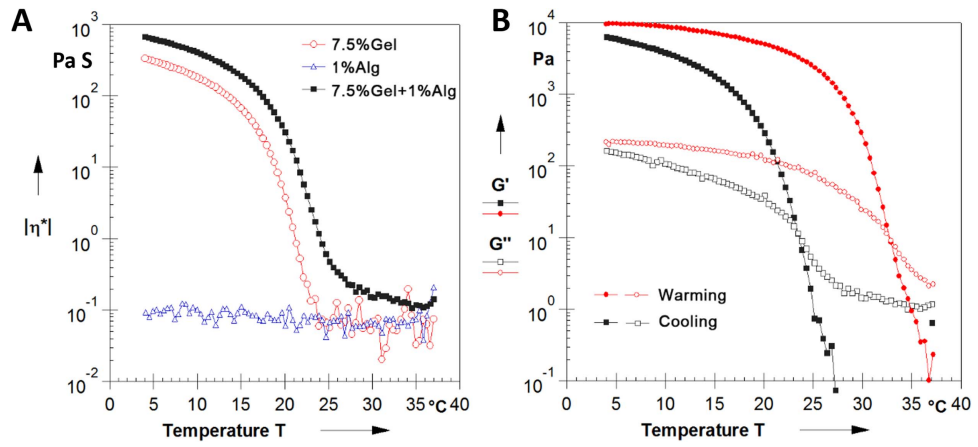

Figure 2. Thermal sensitivity of bioink. (A) Temperature sweep tests indicated complex modulus ($|\eta^*|$) with cooling rate of 5 °C min^{-1} for 7.5% gelatin (7.5%Gel), 1% alginate (1%Alg) and 7.5% gelatin and 1% alginate mixture (7.5%Gel + 1%Alg); (B) Temperature sweep tests indicated storage modulus (G', closed symbol) and loss modulus (G'', open symbol) with warming and cooling rate of 5 °C min^{-1} for 7.5%Gel + 1%Alg bioink.

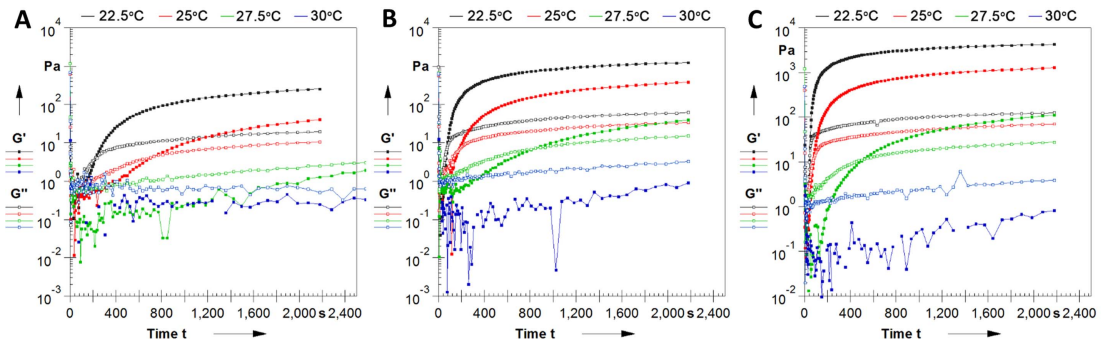

Figure 3. Time sweep tests indicated G' (closed symbol) and G'' (open symbol) under different temperature for (A) 5%Gel + 1%Alg, (B) 7.5%Gel + 1%Alg and (C) 10%Gel + 1%Alg.

(figure 2(B)). The melting temperature in the warming process was about 33 °C, while the gelation temperature in the cooling process was just 24 °C. In addition, the shear rate sweep test of the mixture demonstrated a log-linear relationship between viscosity and shear rate, indicative of shear-thinning properties (figure S2).

Regardless of bioink concentration, the gelatin/alginate bioinks demonstrated time-dependent properties apart from temperature-dependent properties when operating from initial temperature of 37 °C to measurement temperature (22.5 °C~30 °C), as shown in figures 3 and S3. The lower the measurement temperature was, the higher the modulus and viscosity were. It would take a certain time for the gelatin/alginate bioink to get to gelation and then reach a plateau in storage and loss modulus. The time points where G' surpass G'' was recorded as gelation time (t_{gel}), and the complex viscosity at t_{gel} is marked as $|\eta^*|_{gel}$ (figure 4(A)). Figure 4(B) demonstrated a decline in t_{gel} with decreasing temperature. The linear relationship between $\ln(t_{gel})$ and $1/T$ suggested that the temperature-dependent gelation property of gelatin/alginate bioink could be represented by an Arrhenius equation (5) [22]

$$\ln(t_{gel}) = A + \frac{E_a}{RT}, \tag{5}$$

where A is a constant, R is the ideal gas constant (8.314 J K^{-1} mol^{-1} of monomeric units) and T is the measurement temperature (K). According to equation (5), the activation energies (E_a) of 5% Gel + 1%Alg, 7.5%Gel + 1%Alg and 10%Gel + 1% Alg were 424.3 kJ mol^{-1}, 353.5 kJ mol^{-1} and 350.6 kJ mol^{-1}, respectively.

We also examined the relationship between bioink concentration and gelation viscosity, as shown in figure 4(C). Interestingly, even though the gelation time varied at different measurement temperature, gelation viscosity remained on the same level when bioink concentration was constant, suggesting that the gelation viscosity could act as an intrinsic property parameter representing bioink rheology. The gelation viscosity increased from (0.57 ± 0.04) Pa s to (1.84 ± 0.16) Pa s when gelatin concentration increased from 5% to 10% and alginate concentration was fixed at 1%.

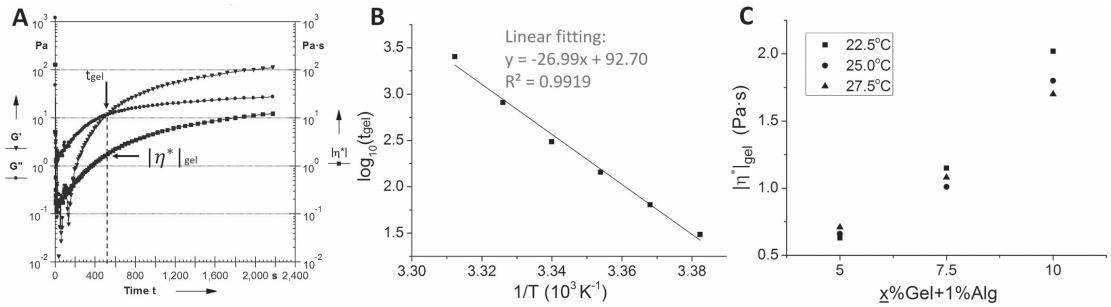

Figure 4. Gelation properties of gelatin/alginate bioink. (A) Representative time sweep test of 10%Gel + 1%Alg bioink at 27.5 °C, demonstrating the gelation time (t_{gel}) and gelation viscosity ($|\eta^*|_{gel}$). (B) Variation of t_{gel} is as a function of temperature. A linear relationship of $\ln(t_{gel})$ versus $1/T$ is fitted. (C) Variation of $|\eta^*|_{gel}$ at different gelatin concentration.

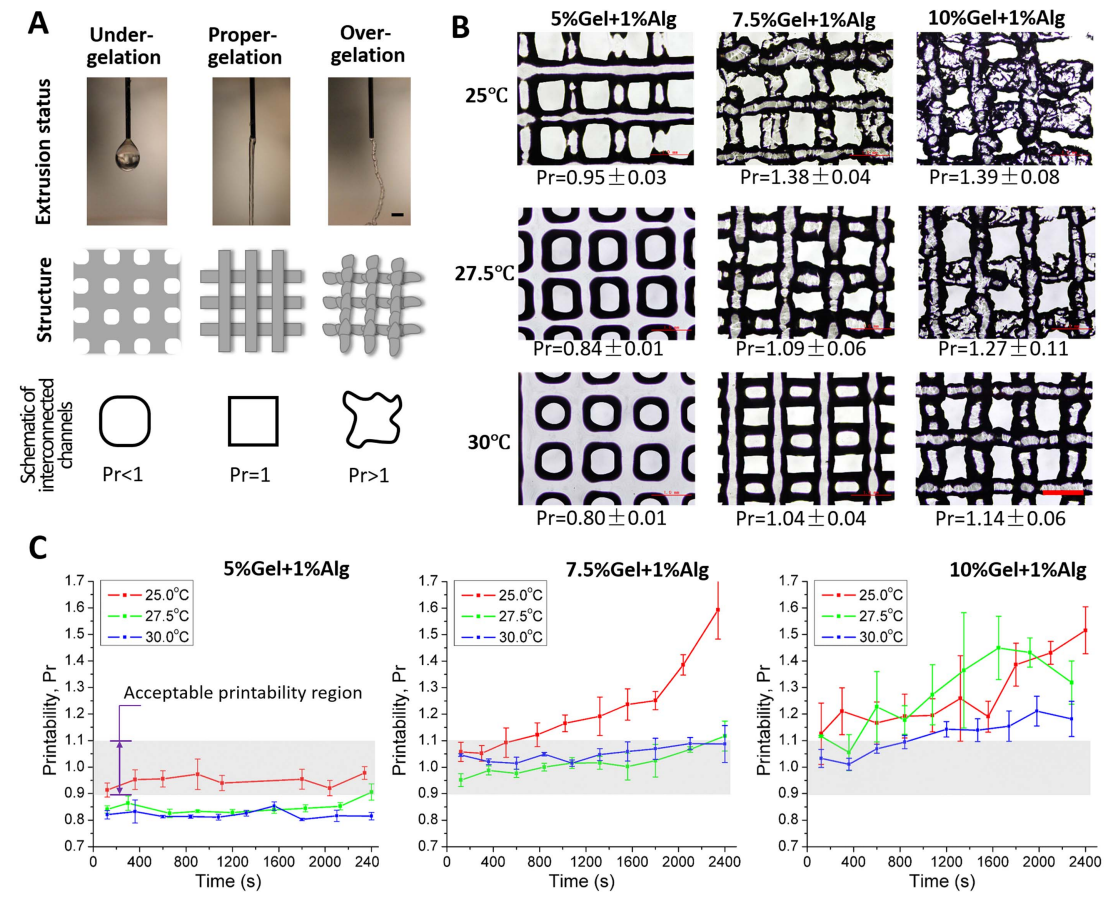

Figure 5. Bioink printability assessment under different printing parameter combinations. (A) Evaluation of printability (Pr) under three typical gelation statuses, namely under-, proper- and over-gelation. (B) Optical microscope images at 30 min. (C) Semi-quantified Pr value of printed construct for gelatin/alginate bioink with different concentrations under different printing temperatures. Scale bars are 1 mm.

3.2. Printability characterization

Bioink printability was assessed using various techniques such as rheology, evaluations of the bioink status on the needle tip, and integrity of printed multilayer construct. There were three gelation statuses for printed bioink: under-gelation, proper-gelation and over-gelation (figure 5(A)). When the bioink was printed with an under-gelation status, it would demonstrate droplet morphology at the nozzle tip (figure 5(A)) and the bioink in a printed construct would fuse on the cross site, making it unfeasible to manufacture a 3D construct with mechanical strength (figure 5(B)). In addition, the formed interconnected channels developed obvious chamfers because of the fusion of the subsequent two layers. When a bioink was printed with the proper-gelation condition, smooth and uniform filaments were extruded continuously, resulting in a standard grid construct with obviously distinguished layers. Furthermore, the morphology of interconnected channels was close to a

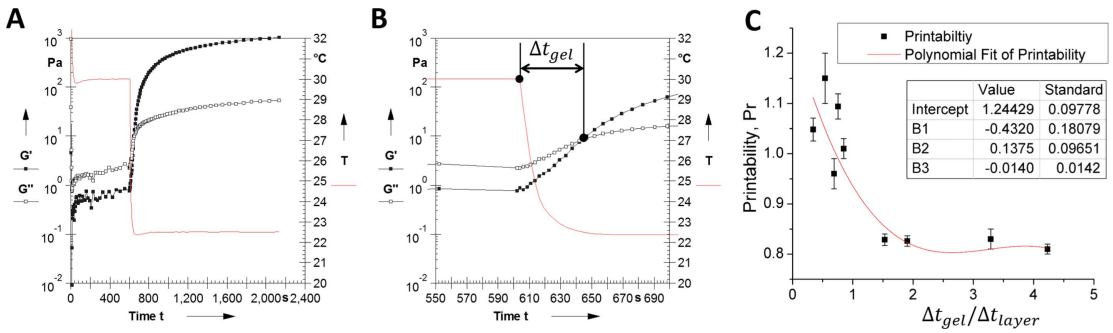

Figure 6. (A) Representative kinetics of gelation of 7.5%Gel + 1%Alg bioink through temperature cycle indicated the response of G' (closed symbol) and G'' (open symbol), and (B) the magnification demonstrated the interval gelation time (Δt_{gel}). (C) The relationship between printability and ratio $\Delta t_{gel}/\Delta t_{layer}$ regardless of gelatin concentration, printing temperature and holding time.

square with regular edges. However, when the bioink had an the over-gelation condition, it would easily show fractured morphology, resulting in irregular of filaments and interconnected channels. In this study, to semi-quantitatively evaluate the bioink printability, a printability characteristic (Pr) was calculated by equation (2) for each parameter combination (figure 5(B)). Based on our experience, when the Pr was in the range of 0.9–1.1, the 3D printed hydrogel construct would demonstrate sound filament morphology and mechanical stability.

Figure 5(C) showed Pr value of gelatin/alginate bioink with different concentrations under different printing temperatures and different holding times. It was demonstrated that printability varied little during the whole holding time for the 5%Gel + 1%Alg bioink. Furthermore, when the printing temperature was 25 °C, printability was within the proper region at all the tested time points. On the other hand, when the printing temperature was 27.5 °C or 30 °C, the Pr was always lower than 0.9, suggesting an under-gelation condition. Referring to the 7.5%Gel + 1%Alg bioink, 27.5 °C and 30 °C were proper printing temperatures during the whole holding process, while 25 °C would result in over-gelation condition after 10 min. These results suggested that when the printing temperature was set at 25 °C for the 7.5%Gel + 1%Alg bioink, the printing process must be completed within 10 min to avoid over-gelation. And this time window is impractical when many constructs, or a construct with large volume, must be printed. As to the 10%Gel + 1%Alg bioink, the Pr increased with holding time at different printing temperatures. When the printing temperature was 25 °C and 27.5 °C, the Pr was higher than 1.1 regardless of holding time, suggesting an over-gelation condition.

During the extrusion process, bioinks went through the temperature change from nozzle insulation temperature (namely printing temperature) to chamber temperature (room temperature of 22.5 °C in this study). The kinetics of bioink gelation through the temperature cycle were studied (figure 6(A)). The bioink responded quickly to the decrease of temperature and initiated gelation from a sol-like status. But it would take a certain time for the bioink to reach gelation point. Here we define this time as Δt_{gel} (figure 6(B)). Figure 6(C) showed the relationship between printability and the ratio $\Delta t_{gel}/\Delta t_{layer}$, where Δt_{layer} is the time for printing between two layers. The results indicated that when the ratio $\Delta t_{gel}/\Delta t_{layer}$ was less than 1, the value of printability was above 0.9.

3.3. Cell viability characterization

Considering the temperature sensitivity of the gelatin/alginate bioink, cells were also incubated at 37 °C and were immediately gently blended with incubated bioink to avoid gelation during the material preparation process. After blending, the cells in the mixture maintained a viability of (97.31 ± 1.61)%, which is higher than that of our previous study (namely, (93.14 ± 1.31)%) [18] with a statistically significant difference (figure S4). Figure 7(A) showed the change of cell viability with different holding time when the 7.5%Gel + 1%Alg bioink was printed at PT-25 °C. In general, cell viability decreased with holding time, especially for higher gelatin concentration and lower printing temperature (figures 7(B)–(D)). There were three combinations of bioink formulation and print temperature that obtained high cell viability (about 90%) within 40 min: 5%Gel + 1%Alg at PT-27.5 °C, 5%Gel + 1%Alg at PT-30 °C and 7.5%Gel + 1%Alg at PT-30 °C.

Shear stress was determined for different gelation concentrations and printing temperatures using the methods stated above and in the supporting information. A simple exponential relationship was observed between cell viability and maximum shear stress (figure 8). Higher shear stresses would result in lower cell viabilities. When shear stress was lower than 100 Pa, a cell viability of more than 90% could be obtained.

3.4. The conjunction of printability and viability

Both printability and viability are influenced by the three parameters considered, namely printing temperature, gelatin concentration and holding time, as

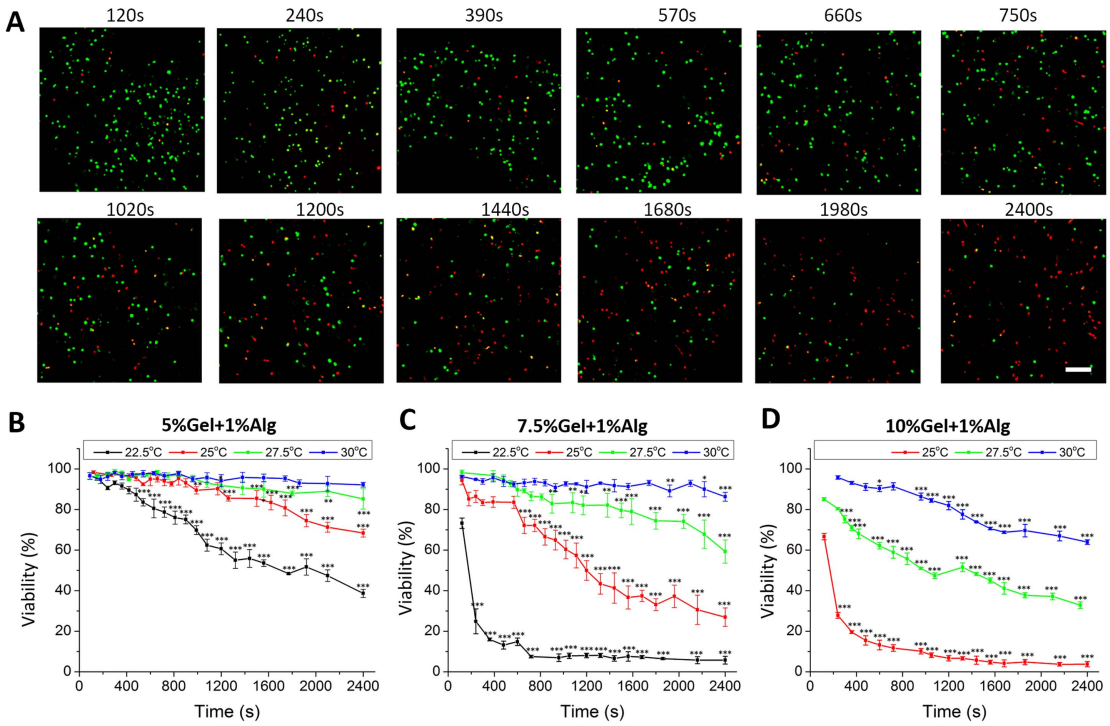

Figure 7. Cell viability evaluation under different printing parameter combinations. (A) Live/dead images showed the viability changed with holding time for 7.5%Gel + 1%Alg at PT-25 °C. (B)–(D) Cell viability as a function of holding time during printing period under different printing temperature for (B) 5%Gel + 1%Alg, (C) 7.5%Gel + 1%Alg and (D) 10%Gel + 1%Alg. Scale bar is 200 μm.

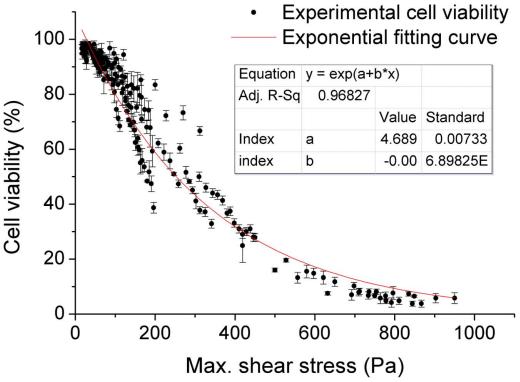

Figure 8. The exponential relationship between cell viability and maximum shear stress by combining all the experimental data under different bioink concentration, printing temperature and holding time.

stated above. In this study, we studied the conjunction of printability and viability based on these original parameters. Figure 9(A) showed that higher gelatin concentration and lower printing temperature contributed to higher printability value. For cell viability, however, lower gelatin concentration and higher printing temperature resulted in higher cell viability (figure 9(B)). At a fixed time point, a correspondingly suitable region of gelatin concentration and printing temperature was generated to achieve suitable printability, where the Pr was in the range of 0.9–1.1 (figure 9(A)). Similarly, a suitable region of printing temperature and gelatin concentration was obtained when the minimum value of cell viability was set at 90% (figure 9(B)). Through combining these two regions generated for printability and cell viability, respectively, a conjunction region was obtained at the overlapped section (figure 9(C)). When applying a gelatin concentration of 7.5% and a printing temperature of 30 °C, which was within the conjunction region, standard multilayered structure (figure 9(D)) and very high cell viabilities (>95%) (figure 9(E)) were obtained. Specifically, it was demonstrated that the cell-laden construct showed high shape fidelity and clear contours, and that ESCs were uniformly distributed in the hydrogel filaments.

4. Discussion

As the most commonly applied 3D cell printing technology, bioplotting dispenses continuous filaments of cell-laden bioink by using pneumatic pressure or motor-driven force, allowing for quickly fabricating large-scale 3D constructs with a wider range of bioink viscosities [1, 23]. However, due to the requirements for extrusion of viscous bioink in harmony with the post-extrusion solidification process, it becomes more complex and challenging for successful 3D printing of living cells because cell viability should be maintained while the bioink is performing a gelation process. Extrusion-based bioplotting technology has been reported to achieve high

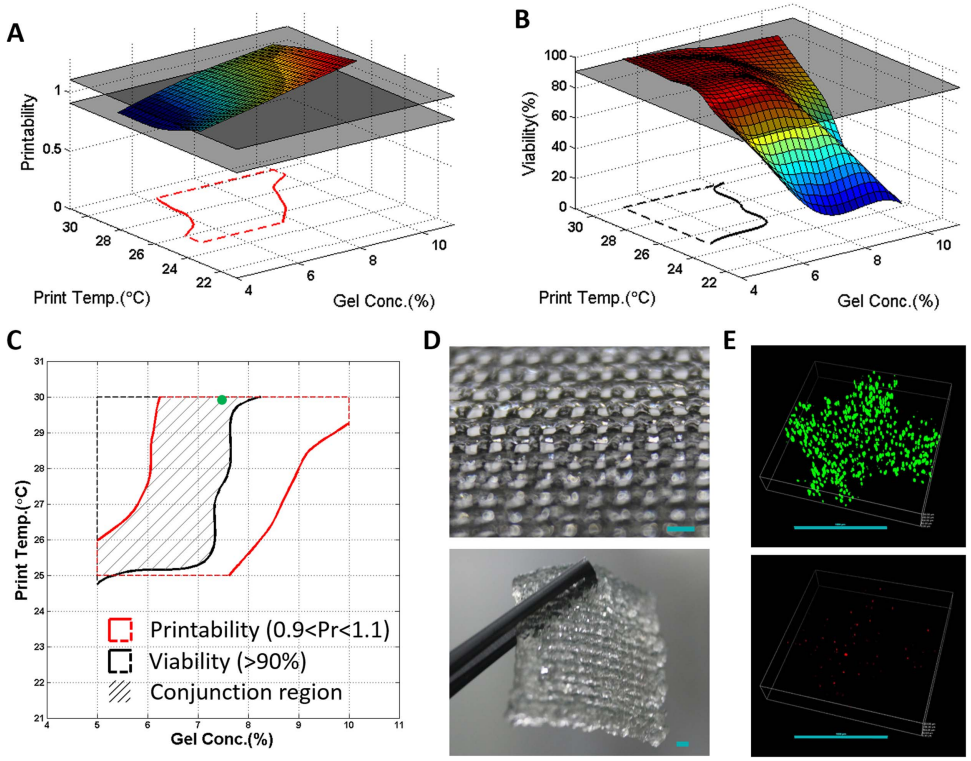

Figure 9. Evaluation and balance of printability and viability under different gelatin concentration and printing temperature combinations, with holding time of 10 min. (A) 3D surface showed printability as a function of gelatin concentration and printing temperature, and a proper range of printability from 0.9 to 1.1 was set to determine the printability region. (B) 3D surface showed viability as a function of gelatin concentration and printing temperature, and viability of more than 90% was set to determine the viability region. The fitting 3D surface of (A) and (B) were obtained by applying the 'surf' function in Matlab. (C) The cross section of printability and viability regions determined the balance region (shaded area). (D) Morphology of printed 3D construct and (E) ESCs live/dead staining were obtained by using the parameter combination within the shaded area (green spot) in (C). Scale bars are 1 mm.

cell viability (>90%) for many types of cells [24–26]. However, a systematic study of construct fabrication and cell viability is needed, especially for some specific cell type, like ESCs.

Gelatin, a soluble protein compound obtained by partial hydrolysis of collagen, has been widely used in wound dressing and other surgical applications [9]. Gelatin demonstrates sol-like status above a gelation temperature, and turns gel-like hydrogel upon cooling because of the formation of conformational cross-bonds [27]. Given its simple thermal-crosslinking property, gelatin has been used as basic cell printing component for more than ten years [4, 28–30]. However, the thermal crosslinking of gelatin is reversible, and the cross-bonds could easily breakdown under physiological conditions. Alginate, isolated from brown algae, has been widely used as cell transplantation vehicles and a matrix material for tissue engineering and controlled drug delivery applications [31]. Alginate gel formation can be quickly achieved through binding by divalent cations and the formed gel is more stable than thermally crosslinked gelatin when cultured in physiological conditions [32]. The gelatin/alginate bioink combines the characteristics of the temperature sensitivity of gelatin to print multi-layered construct and of the rapid ionic crosslinking of alginate for long-term culture [13, 33], and it is commonly used as bioink in cell printing practice [9, 18, 30, 34]. Based on the previous study of bioplotting ESCs with gelatin/alginate hydrogel [12], we chose this mixture as bioink in this study. The robust process is outlined in figure 1, showing the time flow and temperature setting for each step.

To satisfy the rheological requirements for solid filament formation during the extrusion process, the bioink should turn from a sol or under-gelation status to a proper-gelation status when being extruded from the bioink cavity onto the printing platform. Gelatin demonstrated suitable rheological characteristics under temperature sweeps, because an obvious gel transition could be observed when temperature decreased (figure 2). On the other hand, the viscosity of alginate stayed nearly the same under different temperatures (figure 2(A)). Given this, researchers have tried spraying divalent cation solutions to crosslink alginate immediately after extrusion from the nozzle tip or tried extruding pre-crosslinked alginate, which, however, would decrease the stickiness of adjacent layers or decrease the consistency of bioink, respectively [9]. This study demonstrated that the gelatin/alginate mixture showed similar rheology properties to gelatin alone (figure 2(A)). Hence, in the mixture bioink system, gelatin was selected as the major component for construct formation after bioink extrusion into the

printing chamber. Alginate functioned as a stabilizer for the long-term culture by ionic crosslinking under physiological conditions. During the gelation of gelatin, 3D network of fringed micelles was formed, while the generated cross-bonds would be disrupted on heating, which was demonstrated in figure 2(B). However, the gelation point and melting point varied with temperature because the gelatin rheology properties were dependent on thermal history, which brought a time factor into consideration. Therefore, the rheological properties of gelatin/alginate could be tuned through the control over gelatin concentration, temperature and time (figure 3). In addition, it was reported [25] and confirmed in this study (figure S5) that the viscosity of bioink decreased with increasing of cell density. However, there were no significant differences when the cell density was under 2×10^6 cells ml^{-1} (figure S5). Therefore, we used gelatin/alginate bioink to represent the bioink with ESCs of 1×10^6 cells ml^{-1} for rheological studies. Generally, the modulus of the gel increased with holding time since more cross-bonds were formed (figure 4(A)). Under fixed bioink concentration, a decrease in t_{gel} was demonstrated by decreasing the temperature from 30 °C to 22.5 °C (figure 4(B)), meaning it would take longer time to achieve gelation status under higher temperature. With the increase in gelatin concentration, the gelation viscosity ($|\eta^*|_{gel}$) increased regardless of the temperature (figure 4(C)) and this could also be explained by the increase of cross-bonds [27].

As shown in the rheological results, the gelation of gelatin/alginate was a time-dependent process with a theoretical gelation point. As a result, the bioink would demonstrate a slightly different gelation status after being extruded through a needle (figure 5(A)). Generally, if the bioink is in a sol-like or an under-gelation status after printing from the nozzle, it is usually unsuitable for bioplotting, because the mechanical strength of the printed bioink is not enough for supporting the fabrication of a 3D construct. With respect to printability, most reports tried to enhance bioink viscosity to avoid a sol-like or under-gelation status. However, when a bioink was too viscous, the filament would be irregular and unstable because of gel fracture [35]. Given this, we presented a new methodology for assessing printability based on the gelation degree. Fabricating a 3D construct with bioink in a proper-gelation status required a moderate rheological condition that was neither too weak nor too strong. Printability had been assessed using rheology, bioink consistency measurements and measurements of sample dimensions [9]. However, there was no well-accepted definition for printability, and it was difficult to quantify. We noticed that the interconnected channels of the printed construct demonstrated three diacritical profile types under the three gelation statuses. Hence, we introduced a novel approach to semi-quantify printability by analyzing convexity of the interconnected channel profiles, which could be used to discriminate the three types of gelation statuses and to guide the selection of suitable parameters (figures 5(B) and (C)). By defining and semi-quantifying printability, this method can be referred to by other researchers to better characterize bioprinting processes.

In this study, the bioinks experienced a cooling process from a printing temperature (22.5 °C, 25 °C, 27.5 °C and 30 °C) in the nozzle cavity to room temperature (22.5 °C) in the printing chamber, during which the bioinks were desired to turn into gels (figure 6(A)). We hypothesized that the interval time (Δt_{gel}) from the beginning of the temperature dropping to the gelation point, as shown in figure 6(B), would influence the printability. Larger Δt_{gel} meant that it would take longer to achieve gelation once being extruded from the nozzle. When Δt_{gel} was much longer than interval time between printing of two layers (Δt_{layer}), the current layer would not be mechanically strong enough to support the upper layer, resulting in lower printability thus an under-gelation status. In order to avoid an under-gelation status, the ratio $\Delta t_{gel}/\Delta t_{layer}$ should be less than 1, as indicated in figure 6(C).

Cell viability is usually studied together with the rheological characteristics of a bioink, and it is commonly reported that higher viscosity or modulus result in lower cell viabilities [12, 25, 36–38], which was also confirmed in this study. Because of the time-dependent properties of gelatin/alginate mixtures, cell death increased with holding time (figure 7(A)). Despite the rapidity of 3D printing, inferior lower limit of viability should be set for the whole time period of fabrication, taking into consideration this time-dependent behavior. In this study, the time window was set as 40 min. Higher gelatin concentration and lower temperature, which both contributed to strong rheology, would lead to lower cell viability, as demonstrated in figures 7(B)–(D). Actually, for extrusion-based bioplotting technology, cell death and damage could be due to the induced shear stress during extrusion process [10, 15]. Shear stress is determined by bioink viscosity, extrusion speed and nozzle size. When integrating all the cell viability outcomes resulting from different parameter combinations into the same diagram, the rates of viability demonstrated an exponential relationship to induced shear stress (figure 8). That is to say, we experimentally established the relationship between shear stress and cell viability. Although the influence of shear stress on viability might be similar for different cell types, the actual value could be variable because of cell diversity. When applying the same printing parameters (7.5% Gel + 1%Alg with 1 million cells ml^{-1} at PT-22.5 °C), the viability of ESCs ((13.8 ± 2.1)%) was much lower than those of myoblasts ((54.7 ± 3.1)%) and cancer cells ((88.4 ± 2.5)%) with statistically significant differences (figure S6). By using ESCs as a candidate cell

type, this study might be more instructive for the printing of sensitive cells.

Bioink printability and cell viability should be both achieved for successful bioplotting, and this has only been emphasized recently. Ideal gel construct calls for a semi-viscous condition in order to form regular filaments and maintain integrity and shape fidelity, while high cell viability demands the viscosity of the bioink be as low as possible to decrease induced shear stress. In the previous study on A549 cells, the G' of bioink was selected as a criterion for printability and viability characterizations; a G' ranging from 154 Pa to 382 Pa was found to be suitable when using 5%Gel + 1%Alg [14]. Given the cell type differences, in this study on ESCs, we modified the methods to better understand the printing process, as indicated in figure 1. Specifically, (1) an initial temperature (37 °C) was set for all samples considering the thermos-sensitive properties of gelatin-based bioinks; (2) gelatin concentration, holding temperature and time were all systematically studied to precisely locate the suitable parameter configurations; (3) bioink printability was semi-quantified for better analysis and presentation of results; and (4) both bioink printability and cell viability were explained. Here we found that the suitable G' for printing ESCs ranged from 1.38 Pa to 13.7 Pa when using a 5%Gel + 1%Alg bioink (figure S7). In addition, the G' scope differed with gelatin concentration, such that with increasing concentration, the narrower this scope became (figure S7). For more applicable guidelines for ESC printing, we used the original parameters to determine the suitable scope for printability and viability. By setting the proper range for printability and viability, we can obtain the required scope of initial parameters, namely gelatin concentration, printing temperature and holding time (figures 9 and S8). The overlapped region in figures 9(C) and S8(C) presented suitable parameters that can balance printability and viability at a given time point. The results demonstrated that the longer holding time would result in narrower region of printing temperature and gelatin concentration, which confirmed the importance of controlling time for printing gelatin-based bioink. By applying the parameters within the region during whole printing process, multilayer structures (up to twenty layers) can be printed with good fidelity (figures S8(D), (E)).

5. Conclusion

This study systematically investigated the rheological characteristics of a gelatin/alginate mixture with gelatin as a major component for gel formation for bioplotting ESCs under different parameter combinations. Considering the thermo-history dependence and the time-dependent behavior of gelatin/alginate bioinks and sensitivity of ESCs towards induced shear tress, parameters like the bioink concentration, printing temperature and holding time were all taken into account to achieve both good printability and high cell viability. By introducing a semi-quantitative method for assessment of printability, we were able to select a set of suitable process parameter combinations to obtain 3D gelatin/alginate constructs with controlled uniformity as well as to study the viability of ESCs. Specifically, 7.5%Gel + 1%Alg bioink with PT-30 °C was chosen as an optimized parameter combination for the whole printing period. Furthermore, considerations like differences in cell type and the influence of printing time, which were seldom mentioned previously, were emphasized in this study. The novel method developed in this study and the selected process parameter combination might be useful for cell printing studies with different bioinks and cells.

Acknowledgments

The authors thank Dr Jie Na for her kind gift of cell source and Dr Chris Highley for his help in proofreading. This study was funded by the National Natural Science Foundation of China (No. 51235006 and No. 31500818), the Independent Scientific Research Program of Tsinghua University (No. 2014z21030) and the Beijing Municipal Science & Technology Commission Key Project (No. Z1411000002814003).

References

[1] Seol Y J, Kang H W, Lee S J, Atala A and Yoo J J 2014 Bioprinting technology and its applications *Eur. J. Cardio-Thorac.* **46** 342–8
[2] Skardal A and Atala A 2015 Biomaterials for integration with 3D bioprinting *Ann. Biomed. Eng.* **43** 730–46
[3] Mironov V, Boland T, Trusk T, Forgacs G and Markwald R R 2003 Organ printing: computer-aided jet-based 3D tissue engineering *Trends Biotechnol.* **21** 157–61
[4] Yan Y *et al* 2005 Fabrication of viable tissue-engineered constructs with 3D cell-assembly technique *Biomaterials* **26** 5864–71
[5] Demirci U and Montesano G 2007 Single cell epitaxy by acoustic picoliter droplets *Lab Chip.* **7** 1139–45
[6] Barron J A, Wu P, Ladouceur H D and Ringeisen B R 2004 Biological laser printing: a novel technique for creating heterogeneous three-dimensional cell patterns *Biomed. Microdevices.* **6** 139–47
[7] Ouyang L, Highley C B, Rodell C B, Sun W and Burdick J A 2016 3D Printing of shear-thinning hyaluronic acid hydrogels with secondary crosslinking *ACS Biomater. Sci. Eng.* (doi:10.1021/acsbiomaterials.6b00158)
[8] Murphy S V, Skardal A and Atala A 2013 Evaluation of hydrogels for bio-printing applications *J. Biomed. Mater. Res.* A **101** 272–84
[9] Chung J H Y *et al* 2013 Bio-ink properties and printability for extrusion printing living cells *Biomater. Sci.—Uk.* **1** 763–73
[10] Nair K *et al* 2009 Characterization of cell viability during bioprinting processes *Biotechnol. J.* **4** 1168–77
[11] Hendriks J *et al* 2015 Optimizing cell viability in droplet-based cell deposition *Sci. Rep.* **5** 11304
[12] Catros S, Guillotin B, Bacakova M, Fricain J C and Guillemot F 2011 Effect of laser energy, substrate film thickness and bioink viscosity on viability of endothelial cells printed by laser-assisted bioprinting *Appl. Surf. Sci.* **257** 5142–7

[13] Ouyang L, Yao R, Chen X, Na J and Sun W 2015 3D printing of HEK 293FT cell-laden hydrogel into macroporous constructs with high cell viability and normal biological functions *Biofabrication* **7** 015010
[14] Zhao Y, Li Y, Mao S, Sun W and Yao R 2015 The influence of printing parameters on cell survival rate and printability in microextrusion-based 3D cell printing technology *Biofabrication* **7** 045002
[15] Blaeser A, Campos D F D, Puster U, Richtering W, Stevens M M and Fischer H 2016 Controlling shear stress in 3D Bioprinting is a key factor to balance printing resolution and stem cell integrity *Adv. Healthc. Mater.* **5** 326–33
[16] Watanabe K *et al* 2007 A ROCK inhibitor permits survival of dissociated human embryonic stem cells *Nat. Biotechnol.* **25** 681–6
[17] Yao R *et al* 2014 Hepatic differentiation of human embryonic stem cells as microscaled multilayered colonies leading to enhanced homogeneity and maturation *Small* **10** 4311–23
[18] Ouyang L, Yao R, Mao S, Chen X, Na J and Sun W 2015 Three-dimensional bioprinting of embryonic stem cells directs high-throughput and highly uniformed embryoid body formation *Biofabrication* **7** 044101
[19] Yao R, Zhang R, Luan J and Lin F 2012 Alginate and alginate/gelatin microspheres for human adipose-derived stem cell encapsulation and differentiation *Biofabrication* **4** 025007
[20] Yao R, Zhang R, Lin F and Luan J 2012 Injectable cell/hydrogel microspheres induce the formation of fat lobule-like microtissues and vascularized adipose tissue regeneration *Biofabrication* **4** 045003
[21] Tropea C, Yarin A L and Foss J F 2007 *Springer Handbook of Experimental Fluid Mechanics* (Berlin: Springer)
[22] Fatimi A, Tassin J F, Turczyn R, Axelos M A and Weiss P 2009 Gelation studies of a cellulose-based biohydrogel: the influence of pH, temperature and sterilization *Acta Biomater.* **5** 3423–32
[23] Ozbolat I T and Yu Y 2013 Bioprinting toward organ fabrication: challenges and future trends *IEEE Transac. Biomed. Eng.* **60** 691–9
[24] Yu Y, Zhang Y, Martin J A and Ozbolat I T 2013 Evaluation of cell viability and functionality in vessel-like bioprintable cell-laden tubular channels *J. Biomech. Eng.* **135** 91011
[25] Billiet T, Gevaert E, De Schryver T, Cornelissen M and Dubruel P 2014 The 3D printing of gelatin methacrylamide cell-laden tissue-engineered constructs with high cell viability *Biomaterials* **35** 49–62
[26] Irvine S A *et al* 2015 Printing cell-laden gelatin constructs by free-form fabrication and enzymatic protein crosslinking *Biomed. Microdevices* **17** 16
[27] Panouille M and Larreta-Garde V 2009 Gelation behaviour of gelatin and alginate mixtures *Food Hydrocol.* **23** 1074–80
[28] Yao R, Zhang R J, Yan Y N and Wang X H 2009 *In vitro* angiogenesis of 3D tissue engineered adipose tissue *J. Bioact. Compat. Pol.* **24** 5–24
[29] Imani R, Emami S H, Moshtagh P R, Baheiraei N and Sharifi A M 2012 Preparation and characterization of agarose-gelatin blend hydrogels as a cell encapsulation matrix: an *in-vitro* study *J. Macromol. Sci.* B **51** 1606–16
[30] Zehnder T, Sarker B, Boccaccini A R and Detsch R 2015 Evaluation of an alginate-gelatine crosslinked hydrogel for bioplotting *Biofabrication* **7** 025001
[31] Augst A D, Kong H J and Mooney D J 2006 Alginate hydrogels as biomaterials *Macromol. Biosci.* **6** 623–33
[32] Jeon O, Alt D S, Ahmed S M and Alsberg E 2012 The effect of oxidation on the degradation of photocrosslinkable alginate hydrogels *Biomaterials* **33** 3503–14
[33] Zhao Y *et al* 2014 Three-dimensional printing of Hela cells for cervical tumor model *in vitro Biofabrication* **6** 035001
[34] Liu H X, Li S J and Yan Y N 2011 Cell direct assembly technology adopting hybrid of gelatin-based hydrogels *Adv. Mater. Res.—Switz.* **189-193** 2986–92
[35] Drury J L and Mooney D J 2003 Hydrogels for tissue engineering: scaffold design variables and applications *Biomaterials* **24** 4337–51
[36] Rizzuto E, Musaro A, Catizone A and Del Prete Z 2009 Measuring tendon properties in mdx mice: cell viability and viscoelastic characteristics *J. Biomech.* **42** 2243–8
[37] Rodriguez M A, Lopez-Lopez M T, Duran J D, Alaminos M, Campos A and Rodriguez I A 2013 Cryopreservation of an artificial human oral mucosa stroma. a viability and rheological study *Cryobiology* **67** 355–62
[38] Kong H 2003 Designing alginate hydrogels to maintain viability of immobilized cells *Biomaterials* **24** 4023–9